

Kondo entanglement in the quasi-two-dimensional heavy fermion compound CeSb₂

Yun Zhang,^{*} Xuebing Luo,^{*} Wei Feng, Shiyong Tan, Qunqing Hao, Qiang Zhang, Dengpeng Yuan, Bo Wang, Yi Liu, Qin Liu, Xiyang Wang, Lizhu Luo, Xiegang Zhu,[†] Qiuyun Chen^{✉,†} and Xinchun Lai^{✉,†}
Science and Technology on Surface Physics and Chemistry Laboratory, Mianyang 621907, China



(Received 14 April 2022; revised 1 July 2022; accepted 11 July 2022; published 22 July 2022)

In the heavy fermion system, development of the Kondo coherence usually occurs as a crossover behavior. However, accurate definition of the onset temperature for complete formation of the heavy quasiparticles is to some extent controversial. Here, the electronic structure of the quasi-two-dimensional Kondo lattice CeSb₂ has been studied by high resolution angle-resolved photoemission spectroscopy (ARPES) and dynamical mean-field theory approach combined with density functional theory. A heavy quasiparticle band, which originates from the hybridization between *f* electrons and conduction electrons, has been observed directly. Moreover, temperature-dependent electronic structure study reveals a transition from high-temperature local spins to low-temperature itinerant electrons in CeSb₂ and the onset temperature of the hybridized *c-f* spectral weight revealed by laser-ARPES is consistent with the crossover temperature from transport and magnetic measurements. Our findings are essential for a microscopic understanding of different energy scales in the heavy fermion system and demonstrate the probability of laser-ARPES in studying the bulk *4f*-electron properties of Ce-based compounds.

DOI: [10.1103/PhysRevB.106.045133](https://doi.org/10.1103/PhysRevB.106.045133)

I. INTRODUCTION

Single ion Kondo effect in a metal host has been well revealed and its characteristic energy scale can be ascribed to the Kondo temperature (T_K), below which the local moments in the single ion are screened by the conduction electrons [1]. However, when a dense array of magnetic moments surrounded by the conduction electron sea [2,3] forms in a compound, the so-called Kondo lattice systems, the situation becomes more complicated and many exotic properties emerge, such as unconventional superconductivity, quantum critical transition, and so on. It is widely believed that there is a localized to itinerant transition of the *f* electrons when temperature decreases in the heavy fermion (HF) systems [4,5]. Traditionally, the localized-itinerant transition temperature, or the so-called coherent temperature (T^*), can be determined by the thermodynamic, transport, magnetic, or spectral measurements and the coherent temperatures revealed by different techniques are in a sense consistent with each other [6]. However, recent high-resolution angle-resolved photoemission spectroscopy (ARPES) studies of some HF systems found that the onset temperature (T^{ARPES}) of the emergence of *f* spectral weight is much higher than T^* [4,7–10]. The discrepancy of the above two different energy scales (T^* and T^{ARPES}) raises two open questions: (1) What do the two energy scales really represent? (2) Which temperature is the real onset temperature of the *c-f* hybridization? More experimental and theoretical research is needed to fully understand these issues.

In the Kondo lattice systems, a category of quasi-two-dimensional rare-earth dantimonides ReSb₂ is reported possessing many interesting properties, such as charge density wave transition, superconductivity, and so on [11,12]. In these compounds, CeSb₂ is the ideal material to study *c-f* hybridization because the only *f* electron in CeSb₂ makes it simpler than other rare-earth dantimonides when considering the interaction between conduction electrons and *f* electrons. CeSb₂ is also an excellent platform to study magnetism. At ambient pressure, it has several magnetic transition temperatures as follows: 15.5, 11.5, 9.5, and 6.5 K, which corresponds to the paramagnetic-magnetically ordered (MO) state, MO-antiferromagnetic (AFM), AFM-AFM, and AFM-ferromagnetic transitions, respectively. By applying pressure, another transition from ferromagnetic state to nonmagnetic state appears [13,14]. Whether there is any interaction between magnetism and the HF state in this *f*-electron compound is still unknown. ARPES is a powerful tool to illustrate this issue, which can detect the electronic structure of both the HF state and magnetism at the same time. However, up to now, systematic ARPES study of CeSb₂ is still lacking.

The crystal structures of rare-earth dantimonides are highly anisotropic for crystallizing in the layered orthorhombic structure and should be easily cleaved. However, due to the loose and chaotic atomic layer lying on the surface after cleaving [12], it is difficult to obtain their accurate surface electronic structures. Thus these compounds are rarely studied by ARPES or scanning tunneling microscopy (STM). Bulk sensitive electronic-structure-study techniques are helpful to study the detailed electronic structures of those compounds, such as soft x-ray ARPES or laser ARPES. However, the energy resolution of soft x-ray ARPES measurements is about 100 meV, which is insufficient to detect the fine structures of

^{*}These authors contributed equally to this work.

[†]Corresponding authors: zhuxg02@gmail.com; chenqiuyun@caep.cn; laixinchun@caep.cn

f states, typically within the energy scale of $k_B T^*$ [15,16]. Laser ARPES is ideal to explore such small dispersions due to its remarkably high resolution, and especially it is more bulk sensitive.

Here we report a combined electronic structure study of the Kondo lattice CeSb_2 by synchrotron radiation ARPES, laser ARPES, and density functional theory (DFT) plus dynamical mean-field theory (DMFT) calculations. The hybridized c - f state is clearly observed with both synchrotron radiation and laser ARPES measurements. Temperature-dependent experiments clearly reveal the localized-itinerant transition of the f electrons and the T^{ARPES} of CeSb_2 by laser ARPES is consistent with its coherent temperature T^* . Our findings give a microscopic understanding of the electronic structure of the CeSb_2 compound and provide the feasibility of laser ARPES to study the bulk $4f$ electrons of Ce-based compound.

II. EXPERIMENT

High-quality single crystals of CeSb_2 were grown by the self-flux method. Chemical compositions of the single crystals were determined by energy dispersive spectroscopy (EDS). X-ray diffraction (XRD) measurements were performed on a PANalytical X'Pert Pro diffractometer ($\text{Cu } K_\alpha$ radiation). Resistivity and magnetism measurements were performed with the Quantum Design Physical Property Measurement System (PPMS). ARPES data in Figs. 2 and 3 were collected at the ‘‘Dreamline’’ beamline of the Shanghai Synchrotron Radiation Facility (SSRF) with a Scienta D80 analyzer. The energy resolution is 17 meV and the angle resolution is 0.2° . The ARPES data in Fig. 4 were obtained at the 6-eV-laser end station with a VG Scienta R4000 photoelectron analyzer. The combined energy resolution is 3 meV or better, and the momentum resolution is better than 0.006 \AA^{-1} . Before performing laser ARPES experiments, the in-plane orientations of CeSb_2 samples were determined with a Laue diffractometer. Before performing ARPES measurements, samples were cleaved *in situ* parallel to the (001) surface in the ultrahigh vacuum condition at 25 K. Base pressures of both systems are below 5×10^{-11} mbar during the whole measurements. For theoretical calculations, we adopt the charge self-consistent version of DFT plus embedded-DMFT approach, as implemented in Haule’s code [17], to investigate the correlation effects on temperature evolution of the electronic structure of CeSb_2 . For the DFT part, the WIEN2K package [18] was used. The Perdew-Burke-Ernzerhof (PBE) functional [19] was adopted to approximate the exchange-correlation functional. The spin-orbital coupling was included in a second-order variational manner. To ensure the convergence of physical quantities, a mesh of $27 \times 27 \times 6$ was used for the integration over the Brillouin zone within the modified tetrahedron method [20]. The basis set size was controlled by $R_{\text{MT}}K_{\text{MAX}} = 8.0$, while for the DMFT part, we adopt $U = 6.0 \text{ eV}$ and $J = 0.7 \text{ eV}$ for describing correlations in the $4f$ orbital, which has been used successfully in describing several cerium compounds resembling to f -electron behavior in CeSb_2 [21,22]. For the double-counting term, we chose the fully localized limit scheme [23] and the initial occupation of f orbital n_f^0 was set to 1. The constructed multiorbital quantum impurity model was then solved using the vertex-corrected one-crossing

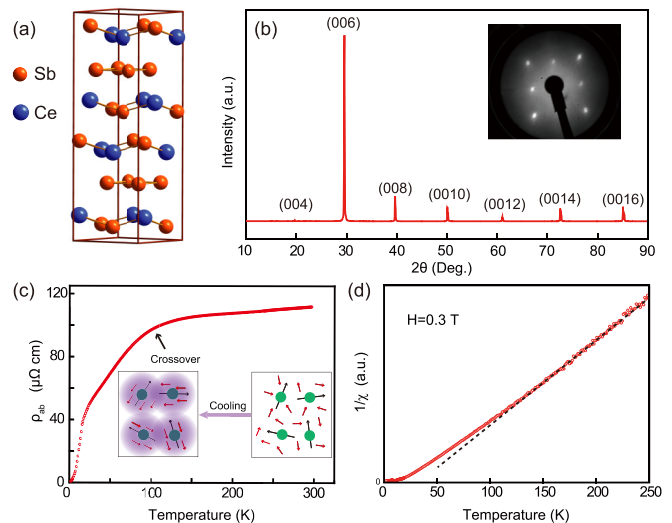


FIG. 1. Crystal structure and physical properties of CeSb_2 . (a) Schematic crystal structure of CeSb_2 with lattice constants of $a = 0.63 \text{ nm}$, $b = 0.61 \text{ nm}$, $c = 1.82 \text{ nm}$ [27]. (b) XRD pattern for the as-grown facet of CeSb_2 single crystals, with (001) diffraction peaks observed exclusively. The inset is the low energy electron diffraction (LEED) pattern of the cleaved surface of CeSb_2 . (c) Temperature dependence of the resistivity of CeSb_2 . The black arrow represents the crossover region around T^* . The inset is the schematic of the localized-itinerant transition of the Kondo lattice systems as a function of temperature. The black and red arrows represent the f electrons and conduction electrons, respectively. The shadow represents the formation of the heavy quasiparticles. (d) Inverse magnetic susceptibility of CeSb_2 as a function of temperature with an applied magnetic field of 0.3 T. The susceptibility data at high temperature is fitted by the Curie-Weiss formula (black dashed line).

approximation (OCA) [24] as the solver. The combination of the DFT and DMFT introduced two self-consistent loops which were repeated until the convergence condition was satisfied. Based on the converged charge and self-energy, the momentum-resolved single-particle spectral function $A(\mathbf{k}, \omega)$ and finite-temperature two-dimensional Fermi surface at $k_z = 0$ plane were obtained with the same recipe as adopted in Ref. [25]. To obtain the Fermi surface at finite T , the quasiparticle approximation was adopted by computing the DFT + DMFT eigenvalues ε_{kl} (l denotes the orbital character) at zero frequency limit $\varepsilon_{kl}(\omega = 0)$ and setting its imaginary part as zero. Therefore the Fermi surface was defined as k points satisfying $\text{Re}[\varepsilon_{kl}(\omega = 0) - \mu] = 0$. In our calculations, the crystal structure parameters referred to a record in the SpringerMaterials database [26].

III. RESULTS

Figure 1(a) displays the schematic crystal structure of CeSb_2 . The lattice constant c of CeSb_2 is much larger than those of a and b . High quality and orientation of the as-grown facet of CeSb_2 are confirmed by XRD and LEED patterns in Fig. 1(b). The resistivity-temperature curve exhibits an obvious crossover behavior around 100 K in Fig. 1(c). The magnetic spin susceptibility also shows the deviation from high temperature Curie-Weiss behavior at $\sim 100 \text{ K}$ in

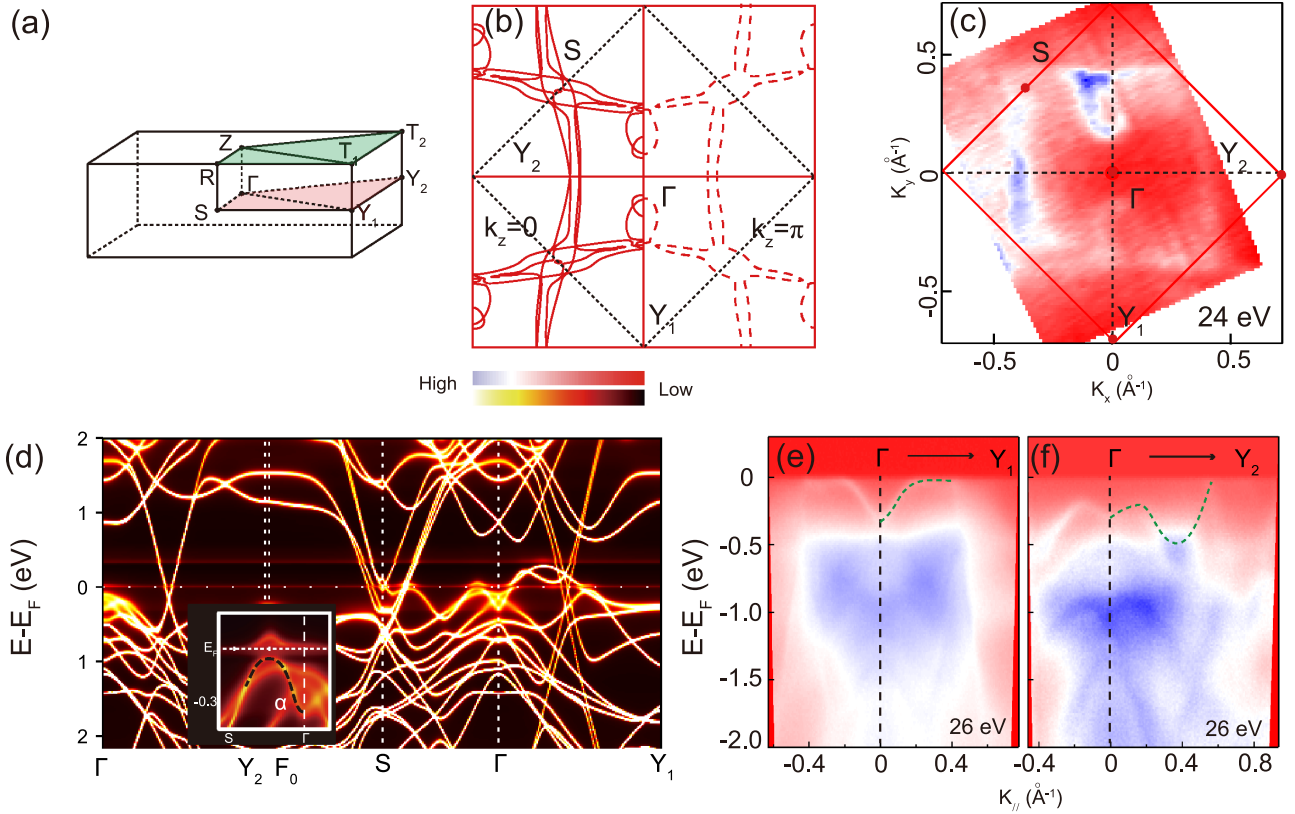


FIG. 2. Fermi surface topology and valence band structure of CeSb₂. (a) Bulk Brillouin zone (BZ) of CeSb₂. The green and pink planes indicate the boundary (Z - R - T , $k_z = \pi$) and center (Γ - S - Y , $k_z = 0$) planes of the BZ of CeSb₂, respectively. (b) Calculated Fermi surface topologies of CeSb₂ at $k_z = 0$ and $k_z = \pi$ planes, respectively. The solid red line in the left panel represents the Fermi surface topology at $k_z = 0$, while the dashed line in the right panel represents the one at $k_z = \pi$. (c) Photoemission intensity map at E_F integrated over a window [$E_F - 10$ meV, $E_F + 10$ meV] of CeSb₂ at 25 K with the photon energy of 24 eV at the “Dreamline” beamline with LH polarized light. (d) Calculated valence band structure of CeSb₂. The inset is the amplified data along the Γ - S direction and the black dashed line denotes the band α . (e),(f) Valence band structure of the CeSb₂ (001) surface along the Γ - Y_1 and Γ - Y_2 directions measured with the photon energy of 26 eV at the “Dreamline” beamline with LH polarized light.

Fig. 1(d), indicating the coherent temperature T^* of CeSb₂ is about 100 K. These indications from resistivity and magnetism measurements have been widely observed in other

f -electron HF materials and are related to the hybridization between local moments and conduction electrons [6,28,29]. At high temperature, the f electrons are localized. With

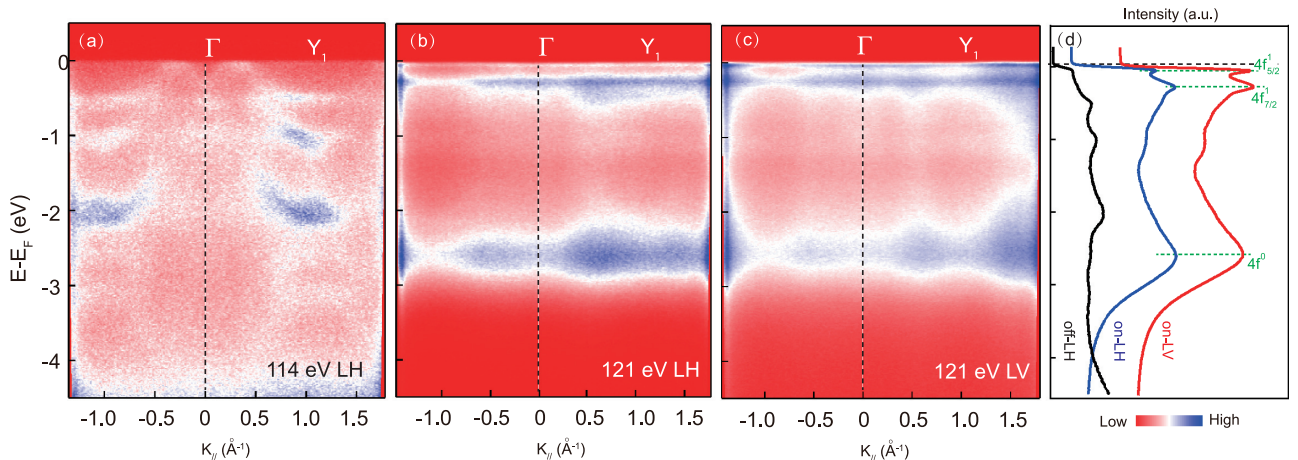


FIG. 3. Photoemission intensity distributions of CeSb₂ along the Γ - Y_1 direction at 25 K with (a) off-resonance (114 eV) LH-polarized photon, (b) on-resonance (121 eV) LH-polarized, and (c) on-resonance (121 eV) LV-polarized photons. (d) Angle-integrated energy distribution curves of CeSb₂ taken with off- and on-resonance photon energy, respectively. f -band positions are highlighted with the green dashed lines.

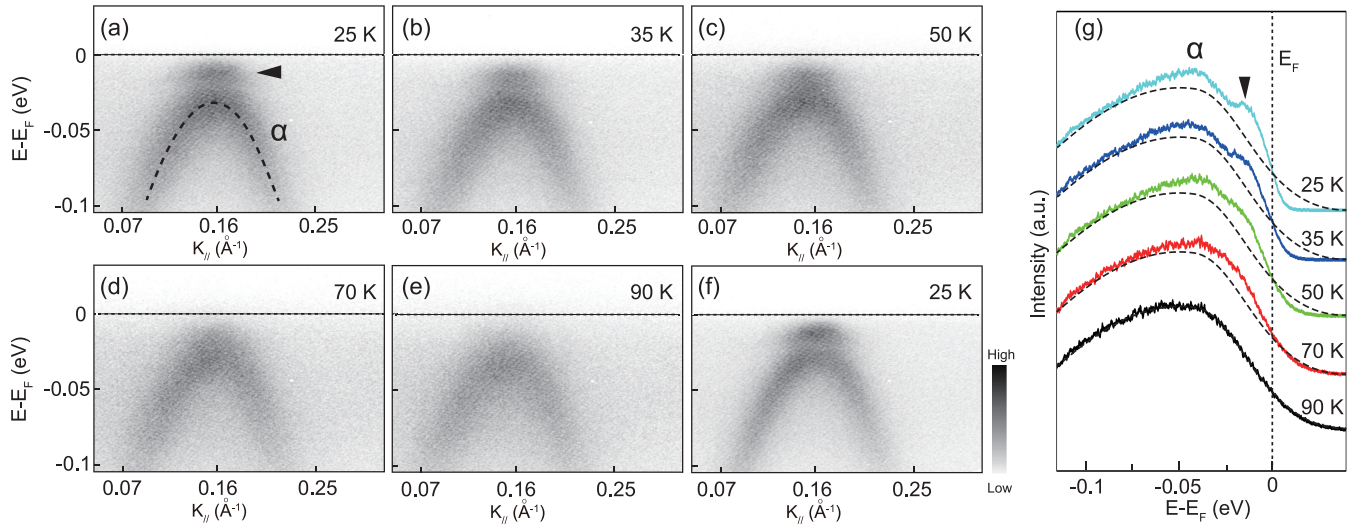


FIG. 4. Temperature dependence of the band structure of CeSb₂ along the Γ - S direction with 6-eV laser ARPES. (a)–(f) Photoemission intensity plots of CeSb₂ along the Γ - S direction as a function of temperature. We warm up the samples from 25 to 90 K (a)–(e) and then cool them down to 25 K (f). The nearly unchanged data quality excludes the possibility of surface aging. (g) Angle-integrated photoemission spectroscopy (AIPES) data of CeSb₂ extracted from (a)–(e). The dashed line is the smoothed AIPES data at 90 K. The black triangle is the mark of f band structure.

decreasing temperature, the f electrons start to hybridize with the conduction electrons accompanied by the formation of heavy quasiparticles as shown in the inset of Fig. 1(c). The Sommerfeld coefficient γ of CeSb₂ measured by specific heat data is about 50 mJ/(mol K²) [12], which is much smaller than other HF compounds, such as CeCoIn₅ and YbRh₂Si₂ [30,31]. The relatively small γ implies that CeSb₂ is a moderate HF compound.

Figures 2(a)–2(c) display the bulk BZ and Fermi surface topologies of CeSb₂. Due to the slight difference between the in-plane lattice constants a and b , the Fermi surface of CeSb₂ has a twofold symmetry in the k_x - k_y plane. At the $k_z = 0$ plane as shown in Fig. 2(b), the topology of the Fermi surface consists of a quasisquarelike pocket centered at the Γ point. Along the Γ - Y_1 direction, there are two eyeball-like pockets, which are missing from the Γ - Y_2 direction, indicating its twofold symmetry. The Fermi surface at the $k_z = \pi$ plane is similar to the one at the $k_z = 0$ plane, as shown in Fig. 2(b). The experimental photoemission intensity map at E_F of CeSb₂ is consistent with the theoretical one, as shown in Fig. 2(c). Both the quasisquarelike pocket and eyeball-like pockets along Γ - Y_1 can be clearly observed. Figure 2(d) shows the calculated valence band structure of CeSb₂ at 20 K. One pronounced character of the band structure is the obvious f weight around the Fermi level. Hybridization between the f electrons and the conduction band can be clearly observed along the Γ - Y_1 and Γ - S directions in Fig. 2(d). The appearance of the f electron states is also confirmed from our experimental data, as shown in Figs. 2(e) and 4. Along the Γ - Y_1 direction, an electron band hybridizes with f electrons around the Γ point near the Fermi level, while along the Γ - Y_2 direction, a hole band is observed around the Γ point with its top at around 0.2 eV binding energy.

To trace the fine structure of f bands, resonant ARPES measurements are conducted at the Ce $4d$ - $4f$ transition edge

to enhance the f -electron photoemission intensity. Comparison of Figs. 3(a) and 3(b) illustrates the enhancement of the f bands by on-resonant condition [Fig. 3(b)]. Strongly dispersive conduction bands dominate the off-resonant data, while three nearly flat bands can be observed in the on-resonant data. The flat band at 2.6 eV binding energy with strong intensity can be assigned to the initial $4f^0$ state, while those near E_F and at 0.29 eV binding energy are attributed to the $4f_{5/2}^1$ state and its spin-orbit-split $4f_{7/2}^1$ component, respectively. As it turns out, the $4f_{5/2}^1$ state is sensitive to the polarization of the light. A significant enhancement is observed under linear vertical (LV)-polarized light compared with linear horizontal (LH) polarization [Fig. 3(c)]. In contrast, the overall features of the $4f_{7/2}^1$ and $4f^0$ states seem to be insensitive to the polarization. The existence of the $4f_{5/2}^1$ state also implies the hybridization between f electrons and conduction electrons.

Due to extremely high energy resolution and bulk sensitive properties, laser ARPES is a great tool to detect detailed bulk electronic structures. In order to trace the evolution of the f spectral weight accurately, we conducted temperature-dependent 6-eV laser ARPES measurements on CeSb₂, as shown in Fig. 4. Figures 4(a)–4(f) display the valence band structure of CeSb₂ along Γ - S as a function of temperature. At the lowest temperature in Figs. 4(a) or 4(f), the holelike band α can be clearly observed along the Γ - S direction, and another weak spectral weight, which is located at -12 meV (marked by the black triangles), is also visible. This relatively weak spectral weight is located at the similar position with the calculated hybridized c - f band in Fig. 2(d) and can also be found in other f -electron materials [32,33], which suggests that it is probably from the mixing of the orbital character of the conduction band into the f -electron resonance (or its side bands) due to hybridization, namely the hybridized c - f state. The weakness of the spectral weight may be due to

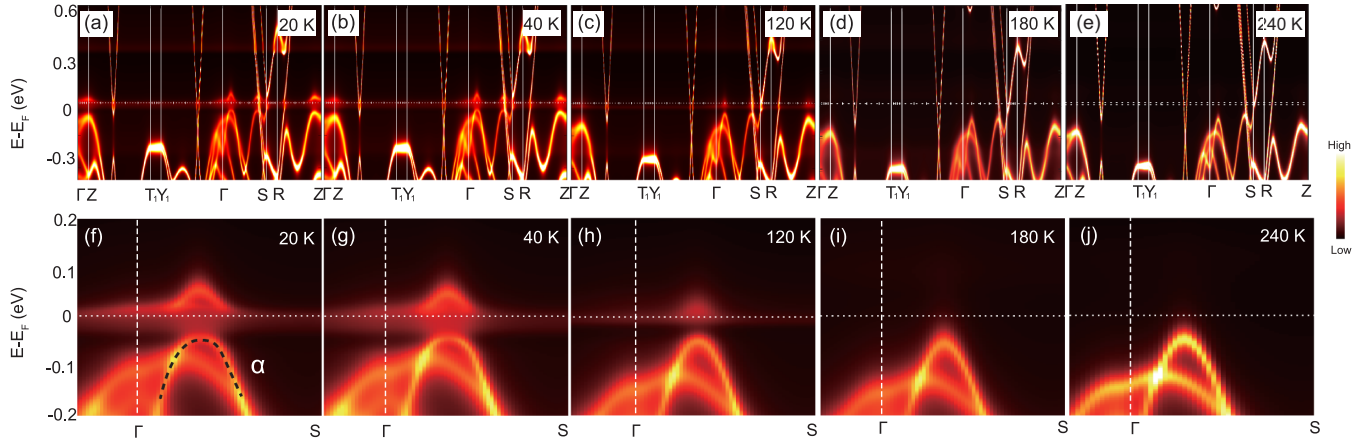


FIG. 5. Calculated temperature dependent band structure of CeSb₂. (a)–(e) Electronic structure of CeSb₂ at five selected temperatures with DFT + DMFT approach. (f)–(j) Amplified data of panels (a)–(e) along the Γ -S direction.

small photoemission cross section of the photons when we use the laser resource (6 eV) to excite the photoelectrons. The photoemission cross section of the Ce 4*f* orbitals is approximately one or two orders of magnitude smaller than the other conduction orbitals, such as Ce (5*d*) and Sb (5*p*) [34]. But other factors that will influence the intensities cannot be excluded, such as the photon polarization, matrix elements, and so on.

With increasing temperature, one pronounced character of the valence band structure is the broadening and weakening of the *c-f* hybridized spectral weight (marked by the black triangle). When the sample temperature is increased up to 90 K, the *c-f* hybridized spectral weight seems to have totally disappeared in Fig. 4(e), which is due to weakening of the hybridization strength between *f* electrons and conduction electrons. At low temperature, *f* electrons hybridize with the conduction electrons and the heavy quasiparticle band forms around the Fermi level. As the temperature increases, the *f* electrons become more localized and the quasiparticle band weakens and finally disappears. This evolution of the *c-f* hybridized spectral weight as a function of temperature can also be clearly reflected in the angle-integrated photoemission spectroscopy (AIPES) data in Fig. 4(g). Besides, we find that, at low temperature, the *c-f* hybridized band is located below the Fermi level. This phenomenon can explain why the Sommerfeld coefficient of CeSb₂ [~ 50 mJ/(mol K²)] is smaller than other Ce-based HF compounds. The Sommerfeld coefficient γ can be described as follows:

$$\gamma = m^* k_F k_B^2 / 3\hbar^2.$$

Here, m^* is proportional to the density of states (DOS) at E_F . k_F is the Fermi velocity. k_B is the Boltzmann constant and \hbar is the Planck constant. For the CeSb₂ compound, its *c-f* hybridized spectral weight is located slightly below the Fermi level and the DOS at E_F is small as shown in Figs. 4(a) and 4(g). This situation is quite similar to the antiferromagnetic HF compound USb₂, whose *f* band is also below the Fermi level and Sommerfeld coefficient is just 25 mJ/(mol K²) [35]. Except for the *c-f* hybridized band, the holelike α band also broadens with increasing temperature. From the temperature-dependent data in Fig. 4, the onset temperature (T^{ARPES}) of

the *c-f* hybridized spectral weight of CeSb₂ is above 70 K and not far from 90 K, which is consistent with the crossover temperature T^* from resistivity and magnetic measurements in Figs. 1(c) and 1(d).

To have a better understanding of the electronic structure evolution with temperature in CeSb₂, we also performed DFT + DMFT calculations as a function of temperature in Fig. 5. The dispersive α band along the Γ -S direction can be well reproduced. The most pronounced character of the band structure from calculated results is also the weakening of the *f* spectral weight around the Fermi level with increasing temperature, which results from the decreased hybridization strength between *f* electrons and conduction electrons. This localization of the hybridized band is consistent with the experimental results in Fig. 4, but the theoretical temperature-dependent spectra indicate that the onset temperature of the coherent *f* spectral weight is between 120 and 180 K as shown in Figs. 5(f)–5(j). Above 180 K, the hybridized spectral is totally disappeared and the calculated onset temperature is a little higher than the experimental one. Several factors probably contribute to the difference between the experimental and theoretical results, such as the neglect of the crystal structure parameter changes with different temperature, which may affect the exotic behavior of 4*f* electrons. Besides, the crystal field effect cannot be accurately described by the current DFT + DMFT method, which may influence the electronic structure near E_F . Those results give a direct evidence of the existence of the *c-f* hybridization in CeSb₂, even though its Sommerfeld coefficient is small.

IV. DISCUSSION AND CONCLUSIONS

In *f*-electron systems, there are many energy scales. For single magnetic moment in a metal host, the standard energy scale is the Kondo temperature (T_K), below which the magnetic moment is screened by the conduction electrons. When the magnetic moments form a dense array and surrounded by the conduction electron sea, namely the Kondo lattice system, the moments not only can be screened by the conduction electrons, but also can interact with each other by Ruderman-Kittel-Kasuya-Yosida (RKKY) interaction. In the Kondo lattice system, the *f* electrons can hybridize with

conduction electrons and form the HF state and the energy scale should be the coherent temperature (T^*), below which the HF state emerges. The coherent temperature is quite different from the Kondo temperature in that it reflects the collective behavior of f electrons. For T^* , different experimental techniques usually yield similar values for the same HF compound. Conventional HF coherence temperature T^* is defined as the maximum point in the ρ - T curve, which mainly reflects the bulk properties of materials. However, recent ARPES studies of Ce-based HF systems found that the onset temperature (T^{ARPES}) of the emergence of f spectral weight is much higher than the coherent temperature T^* [4,6–10]. We know the f -electron behavior in the HF system on the surface is different from the bulk one [36]. Surface effect may be one of the reasons for this discrepancy. Previously, the photon energies used for the determination of T^{ARPES} are usually in the range 21.2–122 eV. In the photoelectric process, the electrons' inelastic mean free path in solids in this photon energy range is less than 1 nm or 2 monolayers [37], which makes the results easier to be affected by the surface, while the inelastic mean free path of electrons with laser resource is about 3–5 nm or 6–20 monolayers and the detected photoemission signals are much more bulk sensitive [37]. Previously, laser ARPES measurements have been performed on several HF systems, such as URu₂Si₂ and YbRh₂Si₂ [38,39], and the f -electron behaviors are clearly exhibited. Especially, the T^{ARPES} of YbRh₂Si₂ determined by the laser resource is consistent with its T^* [6], while the T^{ARPES} determined from more surface sensitive measurement is much higher than its T^* [9], further emphasizing the surface effect when considering the f weight evolution. Previously, 7-eV-laser ARPES measurements have also been performed in the Ce-based HF compound CeSb [40]. Unfortunately, due to the small $4f$ photoionization cross section, the f electron state is unable to be distinguished. Here our results demonstrate the possibility of detecting the hybridized c - f states in

CeSb₂ by 6-eV-laser ARPES and we also find that the onset temperature (T^{ARPES}) of the emergence of f spectral weight of CeSb₂ is more consistent with its coherent temperature. The detection of the hybridized c - f state by 6-eV-laser ARPES may result from the matrix element effect. Recently some ARPES measurements on Ce-based compounds with different terminations also illustrate the importance of surface or bulk condition when considering the properties of c - f hybridization [41–43]. These results bring into reach the ultimate goal of quantitatively testing many-body theories that link spectroscopy and transport properties, for both the bulk and the surface, separately.

To summarize, we have performed high resolution ARPES measurements and DFT + DMFT calculations to reveal the band structure of the two-dimensional Kondo lattice CeSb₂. Direct hybridization between the f electrons and conduction electrons is clearly observed. Temperature-dependent laser ARPES experiments reveal the localized-itinerant transition of the f electrons. The onset temperature of the hybridized c - f spectral weight by bulk sensitive laser ARPES is consistent with the crossover temperature from resistivity and magnetic measurements. Our findings prove essential for a microscopic understanding of the intricate properties of CeSb₂ compound and exhibit the feasibility to study the Ce-based compound with laser ARPES.

ACKNOWLEDGMENTS

This work was supported by the National Natural Science Foundation of China (Grants No. 11904334, No. 12122409, No. 11874330, No. 11774320, No. 12004349, and No. 11904335), the National Key Research and Development Program of China (Grants No. 2021YFA1601100, No. 2017YFA0303104, and No. 2016YFA0300200), and the ARPES beam line of Shanghai Synchrotron Radiation Facility (SSRF, China).

-
- [1] A. C. Hewson, *The Kondo Problem to Heavy Fermions* (Cambridge University Press, Cambridge, UK, 1997), Vol. 2.
- [2] P. Christian, Superconducting phases of f -electron compounds, *Rev. Mod. Phys.* **81**, 1551 (2009).
- [3] Q. Si and F. Steglich, Heavy fermions and quantum phase transitions, *Science* **329**, 1161 (2010).
- [4] Q. Y. Chen, D. F. Xu, X. H. Niu, J. Jiang, R. Peng, H. C. Xu, C. H. P. Wen, Z. F. Ding, K. Huang, L. Shu, Y. J. Zhang, H. Lee, V. N. Strocov, M. Shi, F. Bisti, T. Schmitt, Y. B. Huang, P. Dudin, X. C. Lai, S. Kirchner *et al.*, Direct observation of how the heavy-fermion state develops in CeCoIn₅, *Phys. Rev. B* **96**, 045107 (2017).
- [5] P. Aynajian, E. H. da Silva Neto, A. Gyenis, R. E. Baumbach, J. D. Thompson, Z. Fisk, E. D. Bauer, and A. Yazdani, Visualizing heavy fermions emerging in a quantum critical Kondo lattice, *Nature (London)* **486**, 201 (2012).
- [6] Y. F. Yang, Z. Fisk, H. O. Lee, J. D. Thompson, and D. Pines, Scaling the Kondo lattice, *Nature (London)* **454**, 611 (2008).
- [7] Q. Y. Chen, D. F. Xu, X. H. Niu, R. Peng, H. C. Xu, C. H. P. Wen, X. Liu, L. Shu, S. Y. Tan, X. C. Lai, Y. J. Zhang, H. Lee, V. N. Strocov, F. Bisti, P. Dudin, J. X. Zhu, H. Q. Yuan, S. Kirchner, and D. L. Feng, Band Dependent Interlayer f -Electron Hybridization in CeRhIn₅, *Phys. Rev. Lett.* **120**, 066403 (2018).
- [8] Q. Y. Chen, C. H. P. Wen, Q. Yao, K. Huang, Z. F. Ding, L. Shu, X. H. Niu, Y. Zhang, X. C. Lai, Y. B. Huang, G. B. Zhang, S. Kirchner, and D. L. Feng, Tracing crystal-field splittings in the rare-earth-based intermetallic CeIrIn₅, *Phys. Rev. B* **97**, 075149 (2018).
- [9] K. Kummer, S. Patil, A. Chikina, M. Güttler, M. Höppner, A. Generalov, S. Danzenbächer, S. Seiro, A. Hannaske, C. Krellner, Y. Kucherenko, M. Shi, M. Radovic, E. Rienks, G. Zwinknagl, K. Matho, J. W. Allen, C. Laubschat, C. Geibel, and D. V. Vyalikh, Temperature-Independent Fermi Surface in the Kondo Lattice YbRh₂Si₂, *Phys. Rev. X* **5**, 011028 (2015).
- [10] Q. Yao, D. Kaczorowski, P. Swatek, D. Gnida, C. H. P. Wen, X. H. Niu, R. Peng, H. C. Xu, P. Dudin, S. Kirchner, Q. Y. Chen, D. W. Shen, and D. L. Feng, Electronic structure and $4f$ -electron character in Ce₂PdIn₈ studied by angle-resolved photoemission spectroscopy, *Phys. Rev. B* **99**, 081107(R) (2019).

- [11] S. L. Bud'ko, P. C. Canfield, C. H. Mielke, and A. H. Lacerda, Anisotropic magnetic properties of light rare-earth diantimonides, *Phys. Rev. B* **57**, 13624 (1998).
- [12] R. F. Luccas, A. Fente, J. Hanko, A. Correa-Orellana, E. Herrera, E. Climent-Pascual, J. Azpeitia, T. Pérez-Castañeda, M. R. Osorio, E. Salas-Colera, N. M. Nemes, F. J. Mompean, M. García-Hernández, J. G. Rodrigo, M. A. Ramos, I. Guillamón, S. Vieira, and H. Suderow, Charge density wave in layered $\text{La}_{1-x}\text{Ce}_x\text{Sb}_2$, *Phys. Rev. B* **92**, 235153 (2015).
- [13] T. Kagayama, Y. Uwatoko, S. L. Bud'ko, and P. C. Canfield, Pressure-induced collapse of ferromagnetism in CeSb_2 , *Phys. B (Amsterdam, Neth.)* **359**, 320 (2005).
- [14] Z. Yun, X. Zhu, B. Hu, S. Tan, D. Xie, W. Feng, Q. Liu, W. Zhang, Y. Liu, H. Song, L. Luo, Z. Zhang, and X. Lai, Anisotropic and mutable magnetization in Kondo lattice CeSb_2 , *Chin. Phys. B* **26**, 067102 (2017).
- [15] S.-i. Fujimori, K. Terai, Y. Takeda, T. Okane, Y. Saitoh, Y. Muramatsu, A. Fujimori, H. Yamagami, Y. Tokiwa, S. Ikeda, T. D. Matsuda, Y. Haga, E. Yamamoto, and Y. Ōnuki, Itinerant $U5f$ band states in the layered compound UFeGa_5 observed by soft x-ray angle-resolved photoemission spectroscopy, *Phys. Rev. B* **73**, 125109 (2006).
- [16] S.-i. Fujimori, T. Ohkochi, I. Kawasaki, A. Yasui, Y. Takeda, T. Okane, Y. Saitoh, A. Fujimori, H. Yamagami, Y. Haga, E. Yamamoto, and Y. Ōnuki, Electronic structures of ferromagnetic superconductors UGe_2 and UCoGe studied by angle-resolved photoelectron spectroscopy, *Phys. Rev. B* **91**, 174503 (2015).
- [17] K. Haule, C.-H. Yee, and K. Kim, Dynamical mean-field theory within the full-potential methods: electronic structure of CeIrIn_5 , CeCoIn_5 , and CeRhIn_5 , *Phys. Rev. B* **81**, 195107 (2010).
- [18] WIEN2k: An Augmented Plane Wave plus Local Orbitals Program for Calculating Crystal Properties (Karlheinz Schwarz, Techn. Universität Wien, Austria, 2001).
- [19] J. P. Perdew, K. Burke, and M. Ernzerhof, Generalized Gradient Approximation Made Simple, *Phys. Rev. Lett.* **77**, 3865 (1996).
- [20] P. E. Blöchl, O. Jepsen, and O. K. Andersen, Improved tetrahedron method for Brillouin-zone integrations, *Phys. Rev. B* **49**, 16223 (1994).
- [21] B. Chakrabarti, M. E. Pezzoli, G. Sordi, K. Haule, and G. Kotliar, Alpha-gamma transition in cerium: Magnetic form factor and dynamic magnetic susceptibility in dynamical mean-field theory, *Phys. Rev. B* **89**, 125113 (2014).
- [22] E. A. Goremychkin, H. Park, R. Osborn, S. Rosenkranz, J.-P. Castellán, V. R. Fanelli, A. D. Christianson, M. B. Stone, E. D. Bauer, K. J. McClellan, D. D. Byler, and J. M. Lawrence, Coherent band excitations in CePd_3 : A comparison of neutron scattering and *ab initio* theory, *Science* **359**, 186 (2018).
- [23] V. I. Anisimov, F. Aryasetiawan, and A. I. Lichtenstein, First-principles calculations of the electronic structure and spectra of strongly correlated systems: The LDA+U method, *J. Phys.: Condens. Matter* **9**, 767 (1997).
- [24] T. Pruschke and N. Grewe, The Anderson model with finite Coulomb repulsion, *Z. Phys. B: Condens. Matter* **74**, 439 (1989).
- [25] H. C. Choi, B. I. Min, J. H. Shim, K. Haule, and G. Kotliar, Temperature-Dependent Fermi Surface Evolution in Heavy Fermion CeIrIn_5 , *Phys. Rev. Lett.* **108**, 016402 (2012).
- [26] https://materials.springer.com/isp/crystallographic/docs/sd_0450241
- [27] R. Wang and H. Steinfink, The crystal chemistry of selected AB_2 rare earth compounds with selenium, tellurium, and antimony, *Inorg. Chem.* **6**, 1685 (1967).
- [28] H. Hegger, C. Petrovic, E. G. Moshopoulou, M. F. Hundley, J. L. Sarrao, Z. Fisk, and J. D. Thompson, Pressure-Induced Superconductivity in Quasi-2D CeRhIn_5 , *Phys. Rev. Lett.* **84**, 4986 (2000).
- [29] P. G. Pagliuso, N. O. Moreno, N. J. Curro, J. D. Thompson, M. F. Hundley, J. L. Sarrao, Z. Fisk, A. D. Christianson, A. H. Lacerda, B. E. Light, and A. L. Cornelius, Ce-site dilution studies in the antiferromagnetic heavy fermions $\text{Ce}_m\text{Rh}_n\text{In}_{3m+2n}$ ($m = 1, 2; n = 0, 1$), *Phys. Rev. B* **66**, 054433 (2002).
- [30] C. Petrovic, P. G. Pagliuso, M. F. Hundley, R. Movshovich, J. L. Sarrao, J. D. Thompson, Z. Fisk, and P. Monthoux, Heavy-fermion superconductivity in CeCoIn_5 at 2.3 K, *J. Phys.: Condens. Matter* **13**, L337 (2001).
- [31] N. Oeschler, S. Hartmann, A. P. Pikul, C. Krellner, C. Geibel, and F. Steglich, Low-temperature specific heat of YbRh_2Si_2 , *Phys. B (Amsterdam, Neth.)* **403**, 1254 (2008).
- [32] H. J. Im, T. Ito, H. D. Kim, S. Kimura, K. E. Lee, J. B. Hong, Y. S. Kwon, A. Yasui, and H. Yamagami, Direct Observation of Dispersive Kondo Resonance Peaks in a Heavy-Fermion System, *Phys. Rev. Lett.* **100**, 176402 (2008).
- [33] M. Klein, A. Nuber, H. Schwab, C. Albers, N. Tobita, M. Higashiguchi, J. Jiang, S. Fukuda, K. Tanaka, K. Shimada, M. Mulazzi, F. F. Assaad, and F. Reinert, Coherent Heavy Quasiparticles in a CePt_5 Surface Alloy, *Phys. Rev. Lett.* **106**, 186407 (2011).
- [34] J. J. Yeh and I. Lindau, Atomic subshell photoionization cross sections and asymmetry parameters: $1 \leq Z \leq 103$, *At. Data Nucl. Data Tables* **32**, 1 (1985).
- [35] Q. Y. Chen, X. B. Luo, D. H. Xie, M. L. Li, X. Y. Ji, R. Zhou, Y. B. Huang, W. Zhang, W. Feng, Y. Zhang, L. Huang, Q. Q. Hao, Q. Liu, X. G. Zhu, Y. Liu, P. Zhang, X. C. Lai, Q. Si, and S. Y. Tan, Orbital-Selective Kondo Entanglement and Antiferromagnetic Order in USb_2 , *Phys. Rev. Lett.* **123**, 106402 (2019).
- [36] L. Jiao, S. Rößler, D. Kim, L. Tjeng, Z. Fisk, F. Steglich, and S. Wirth, Additional energy scale in SmB_6 at low-temperature, *Nat. Commun.* **7**, 13762 (2016).
- [37] M. P. Seah and W. A. Dench, Quantitative electron spectroscopy of surfaces: A standard data base for electron inelastic mean free paths in solids, *Surf. Interface Anal.* **1**, 2 (1979).
- [38] S.-K. Mo, W. Lee, F. Schmitt, Y. Chen, D. Lu, C. Capan, D. Kim, Z. Fisk, C.-Q. Zhang, and Z. Hussain, Emerging coherence with unified energy, temperature, and lifetime scale in heavy fermion YbRh_2Si_2 , *Phys. Rev. B* **85**, 241103(R) (2012).
- [39] R. Yoshida, Y. Nakamura, M. Fukui, Y. Haga, E. Yamamoto, Y. Ōnuki, M. Okawa, S. Shin, M. Hirai, and Y. Muraoka, Signature of hidden order and evidence for periodicity modification in URu_2Si_2 , *Phys. Rev. B* **82**, 205108 (2010).
- [40] Y. Arai, K. Kuroda, T. Nomoto, Z. H. Tin, S. Sakuragi, C. Bareille, S. Akebi, K. Kurokawa, Y. Kinoshita, W. L. Zhang, S. Shin, M. Tokunaga, H. Kitazawa, Y. Haga, H. S. Suzuki, S. Miyasaka, S. Tajima, K. Iwasa, R. Arita, and T. Kondo, Multipole polaron in the devil's staircase of CeSb , *Nat. Mater.* **21**, 410 (2022).

- [41] S. Patil, A. Generalov, M. Güttler, P. Kushwaha, A. Chikina, K. Kummer, T. C. Rödel, A. F. Santander-Syro, N. Caroca-Canales, C. Geibel, S. Danzenbächer, Yu. Kucherenko, C. Laubschat, J. W. Allen, and D. V. Vyalikh, ARPES view on surface and bulk hybridization phenomena in the antiferromagnetic Kondo lattice CeRh_2Si_2 , *Nat. Commun.* **7**, 11029 (2016).
- [42] G. Poelchen, S. Schulz, M. Mende, M. Güttler, A. Generalov, A. V. Fedorov, N. Caroca-Canales, C. Geibel, K. Kliemt, C. Krellner, S. Danzenbächer, D. Yu. Usachov, P. Dudin, V. N. Antonov, J. W. Allen, C. Laubschat, K. Kummer, Y. Kucherenko, and D. V. Vyalikh, Unexpected differences between surface and bulk spectroscopic and implied Kondo properties of heavy fermion CeRh_2Si_2 , *npj Quantum Mater.* **5**, 70 (2020).
- [43] M. Mende, K. Ali, G. Poelchen, S. Schulz, V. Mandic, A. V. Tarasov, C. Polley, A. Generalov, A. V. Fedorov, M. Güttler, C. Laubschat, K. Kliemt, Y. M. Koroteev, E. V. Chulkov, K. Kummer, C. Krellner, D. Yu. Usachov, and D. V. Vyalikh, Strong Rashba effect and different f-d hybridization phenomena at the surface of the heavy-fermion superconductor CeIrIn_5 , *Adv. Electron. Mater.* **8**, 2100768 (2022).